Short-wavelength cone signals contribute to sparse, high-dimensional color tuning in primate OFF midget ganglion cells

Lauren E Wool[1], Orin S Packer[2], Qasim Zaidi[1], and Dennis M Dacey[2*]

1 State University of New York College of Optometry, Graduate Center for Vision Research, New York, NY, (United States); **2** University of Washington, Department of Biological Structure, Seattle, WA, (United States)

*Corresponding author: dmd@uw.edu

Abstract

Primate midget retinal ganglion cells are generally considered the substrate for 'red-green' color signaling and selective for long (L)- and medium (M)-wavelength cone inputs, but anatomical evidence shows OFF midget cells also receive input from the short (S)-wavelength cone. It remains unclear how input from a third cone type affects the color properties of such cells. In this study, we recorded S-cone input to a minority of midget cells (predominantly OFF) in the near peripheral retina, with both L–M opponent and L+M non-opponent OFF midget ganglion cells demonstrating significant spike responses to decrements of S-cone stimuli. The strength of S-cone input was variable in a heterogeneous population of cells that could be characterized as M–(L+S) cone-opponent; L–(M+S) cone-opponent; or –(L+M+S) nonopponent. Our findings strongly support previous anatomical and electrophysiological studies that suggest the midget OFF pathway is the conduit for S-OFF signals in primate retina, and may comprise a sparse network of higher-dimensional color tuning beyond classical L- versus M-cone dynamics.

Keywords

Primate, retina, short-wavelength, cone, color vision, cone-opponency, trichromacy

Introduction

In primate retina, midget ganglion cells are generally considered the substrate for 'red-green' color signaling, as part of trichromatic color vision. A product of antagonistic responses between long (L)– and middle (M)–wavelength cones, the cone opponency exhibited by midget ganglion cells is dependent on a center-surround receptive-field structure, consisting of a receptive-field center driven by direct cone inputs from midget bipolar cells, and a receptive-field surround driven by broad and indiscriminate cone connections to horizontal cells (Crook et al., 2011). So unique is the phenomenon of L–M opponency to midget cells that it is the foundational criterion of their identification as a cell class (Gouras, 1968; De Monasterio and Gouras, 1975); its pervasiveness, especially when considered alongside the overall sparseness of short (S)–wavelength cones in the trichomatic mosaic (Curcio et al., 1991) informs the assumption that the L–M opponent cell class is also—by same design—L- and M- selective.

The presence of L–M opponency across both ON and OFF midget cells has perhaps driven an expectation for a similarly ON-OFF-symmetric, orthogonal "blue-yellow" axis in retina. While the ON circuit of the 'blue-yellow' pathway in primate retina is served by the distinct S cone–selective ON bipolar cell (Mariani, 1984) and the small bistratified "blue ON" ganglion cell (Dacey and Lee, 1994), a similarly dedicated S cone–selective OFF bipolar cell or S-OFF ganglion cell has not been described. However, OFF bipolar–type basal contacts have consistently been observed at the S-cone pedicle (Kouyama and Marshak, 1992; Kolb et al., 1997; Calkins et al., 1998; Calkins, 2000; Lee and Grünert, 2007). Indeed, Klug et al. (2003) showed with electron microscopy that OFF midget bipolar

cells reliably contact S-cone pedicles in macaque fovea—suggesting that transmitting S-OFF signals is another aspect of the midget pathway (the OFF division, at least). This result was recently confirmed and extended using serial blockface scanning electron microscopic reconstructions of macaque money fovea (Dacey et al., 2017). The anatomical results were recapitulated electrophysiologically by Field et al (2010) in the far peripheral retina, who showed that among a population of ON and OFF midget ganglion cells, sensitivity to S-cones was nearly entirely sequestered to OFF cells. Tsukomoto and Omi (2015) also found that OFF midget bipolar cells made variable numbers of basal contacts with S cones in the retinal periphery. As midget cells are known to draw input from multiple cone inputs in the retinal periphery (e.g., (Wool et al., 2018), Figure 1), the authors predicted variable S-cone sensitivity in midget OFF cells as a result of their arrangement alongside other L- and M-cones.

While there is ample evidence to suggest that S-OFF signaling may be an additional feature of the OFF midget circuit, there has been little work done to determine how the color properties of cells in this pathway are altered by S-cone input. If OFF midget cells do indeed receive input from S cones, then their chromatic properties should be more complex than the canonical "red-green" tuning that has historically been ascribed. In this study, we report that S-cone sensitivity is evident in the spiking activity of a small subpopulation of OFF midget cells in the near peripheral retina, forming a sparse, asymmetric counterpart to the S-ON signal carried by small-bistratified 'blue-on' cells. We characterized the strength, sign, and spatial properties of L-, M-, and S-cone input to this population, and found that S-OFF midget cells have a characteristic S-cone spatial signature, but otherwise exhibit heterogeneous color properties across both L–M opponent and nonopponent cells. Our findings thus advance the OFF midget system as a functionally cone-nonspecific and chromatically complex substrate, shaping color tuning beyond that of classical L–M opponency.

Materials & Methods

In vitro *preparation.* Eyes were removed from deeply anesthetized male and female macaque monkeys at the time of euthanasia (*Macaca nemestrina, Macaca fascicularis*, or *Macaca mulatta*) via the Tissue Distribution Program of the Washington National Primate Research Center. After enucleation, the anterior chamber of the eye was removed, the vitreous drained, and the remaining eyecup placed in oxygenated Ames medium (A1420, Sigma). The choroid was then carefully dissected from the sclera so as to maintain intimate contact between neural retina, retinal pigment epithelium and choroid. Radial cuts were made in the isolated retina-choroid to create a flat mount that was adhered, ganglion cell layer up, to the glass bottom of a thermostatically maintained (~36°C, TC-344B, Warner Instruments) steel superfusion chamber coated with poly-L-lysine (P1399, Sigma; 10 mg in 10 mL H_2O). The retina was continuously superfused with Ames' medium (pH 7.37; constant oxygenation with 95% O2/5% CO2; 3–5 ml min^{-1}). Visual stimuli were projected onto the vitreal (ganglion-cell side) of the retina as *in situ*, via the microscope objective lens as described further below.

In vitro *electrophysiology.* Retinal ganglion cells were observed using a 60× water immersion long working distance objective (1.0 NA, Nikon) under infrared illumination. Midget ganglion cells were visually identified and differentiated from other cell types by their relatively high density and small soma size (Dacey and Lee, 1994), which was confirmed by receptive-field mapping: midget ganglion cells showed the smallest center diameters of any primate ganglion cell, 30–150 μm in the near retinal periphery; the other relatively high density ganglion cell types with relatively large cell bodies (parasol and small bistratified cells) show receptive field center diameters ~2-3 times larger than midget cells. Using the 'loose-patch' method, extracellular recordings were made with glass micropipettes (5–8 MΩ) filled with Ames' medium. Data acquisition and stimulus presentation were coordinated by custom software running on an Apple Macintosh computer. Current and spike waveforms were Bessel-filtered at 2 or 5 kHz and sampled at 10 kHz.

Stimulus generation. A digital light projector (Christie Digital Systems) was used to project the visual stimuli (VSG, Cambridge Research Systems) through an optical relay to the microscope camera port and focus the image onto the photoreceptor layer. The irradiance spectra for red, green, and blue primaries were measured with a spectroradiometer (PR705, Photo Research, Inc.); peak wavelengths and integrated photon fluxes were 636, 550, and 465 nm and 2.7×10^6, 6.9×10^5, and 1.8×10^5 photons s^{-1} μm^{-2}, respectively. To compute the effectiveness of the light delivered by each primary to the cone aperture, we calculated the products of each primary irradiance spectrum and each cone spectral sensitivity function (Baylor et al., 1987). We corrected for the spectrally broadening effects of self-screening by assuming a pigment density of 0.016 μm^{-1} (Baylor et al., 1987) and a cone outer segment length of 5 μm: while cones at ~8 mm have an outer segment length of 20 μm (Banks et al., 1991), we correct for the fact that peripheral cones in vitro lay obliquely to the optical axis of the objective, thus shortening the effective path length and reducing light capture. Each product was then summed across wavelength giving units of 'effective' photons s^{-1} μm^{-2} (irradiance corrected by cone spectral sensitivity). Effective photons s^{-1} μm^{-2} were then converted to photoisomerizations s^{-1} $cone^{-1}$ by multiplying by the area of the cone aperture. In previous studies involving transverse illumination of the cone outer segment (Baylor et al., 1979), where funneling of the inner segments plays no role, the conversion factor commonly used is 0.37 μm^2. The efficiency of photoisomerization (0.67) (Dartnall, 1972) is included in this value. In the *in vitro* macaque retina, as *in vivo*, light is incident upon the vitreal surface of the retina and funneling by the inner segment would tend to increase the effective area of the cone aperture. We therefore consider the use of 0.37 μm^2 a very conservative estimate of cone aperture to make the conversion to photoisomerizations s^{-1} $cone^{-1}$.

Often, the intensity of stimuli used in human visual psychophysics or in physiological experiments in the intact primate eye is expressed in units of retinal illuminance, or Trolands (Td). To aid comparison with our data, we previously calculated that for a peripheral cone with an inner segment aperture of 9 μm, 1 Td was equivalent to ~30 photoisomerizations s^{-1} $cone^{-1}$ (Crook et al., 2009).

To achieve cone isolation, both modulation depth and irradiances of the primary lights were adjusted; cone isolation was confirmed by direct recordings from macaque cones and has been reported previously (Packer et al., 2010). Cone contrast was defined as the peak excursion from the background, divided by the mean light level, expressed as a percentage. Computed contrast for cone-isolating stimuli was 18% around a background comprising equal quantal catches for the three cone types. Additional high-contrast S and L+M stimuli were 64% around an equal background. To center the stimulus on the cell's receptive field, the cell body was first placed in the middle of the stimulus field. Fine-diameter horizontal and vertical slits (10 or 25 μm wide) were then systemically moved in the x and y planes to locate the most sensitive point of the receptive field. The location of the maximum spike response was defined as the receptive-field midpoint; stimuli were positioned relative to this point. When possible, the recorded cells' retinal location and distance from the foveal center was determined and recorded as temporal equivalent eccentricity (Watanabe and Rodieck, 1989).

Identifying putative S-cone input and characterizing cone-specific contributions to the receptive field. Retinal ganglion cells were initially surveyed for putative S-cone inputs by recording extracellular spike activity while presenting spots of high-contrast S-cone or (L+M)-cone isolating stimuli to the cell's receptive-field center (150 or 400 μm diameter, 64% contrast), modulated as square waves at 2 Hz temporal frequency. At this frequency, the ON response phase is ~0° and OFF response phase ~180°. Stimulus presentations were repeated 12–20 times and peristimulus time histograms (PSTHs) were constructed from the spikes. PSTHs were then fit with a Fourier series and spiking activity was reported as the amplitude, A, and phase, θ, of the first harmonic (F1). From this spiking activity, S or L+M mechanism-specific responses were classified as either ON or OFF with strength $R = A\cos(\theta)$, where $-R$ denotes an OFF response and $+R$ denotes an ON response. While we always stimulated ganglion cells at photopic light levels to prevent against rod intrusion, this

computation further penalizes any spurious rod response, which has a much longer latency to light increments (~270°; see (Crook et al., 2009) Figure 5D). Cells with both $|R_{L+M}| \leq 3.5$ spikes/s and $|R_S| \leq 3.5$ spikes/s were considered unresponsive and were not included in further analyses. Midget cells with $|R_S| > 3.5$ spikes/s were considered to have putative S-cone input.

To fully characterize the specific L-, M-, and S-cone inputs to individual cells, extracellular spike activity was recorded while presenting full-field L-, M-, or S-cone isolating stimuli (800 or 1200 µm diameter, 18% contrast), modulated as square waves at a temporal frequency of 2 Hz. Stimulus presentations were repeated 12–20 times; PSTHs were constructed and fit with a Fourier series and spiking activity was reported as the amplitude, A, and phase, θ, of the first harmonic (F1). From this spiking activity, cone-specific responses were classified as either ON or OFF with strength $R = A\cos(\theta)$, where $-R$ denotes an OFF response and $+R$ denotes an ON response. To compare the relative strength of L-, M-, and S-cone inputs to each cell, responses were normalized as $\overline{R_L} = R_L/|R_L| + |R_M| + |R_S|$, $\overline{R_M} = R_M/|R_L| + |R_M| + |R_S|$, and $\overline{R_S} = R_s/|R_L| + |R_M| + |R_S|$. For midget cells when the initial high-contrast S or L+M stimulus was not run, we assessed responses to low-contrast stimuli with similar criteria as above to classify cells as unresponsive ($|R_L| \leq 3.5$ spikes/s and $|R_M| \leq 3.5$ spikes/s).

Computing spatial frequency tuning. The spatial tuning of midget-cell receptive fields was characterized using S cone–isolating or (L+M) cone–isolating drifting gratings (modulated at 2 Hz temporal frequency) of varying spatial frequency (spatial frequency 1/32–16 cpd, contrast 56% or 72%). For each cell, spike rate amplitude (A) and phase (θ) were computed from the first Fourier harmonic (F1) at each stimulus frequency, and tuning curves were constructed from pairs of amplitude/phase measurements at each spatial frequency. Tuning curves were then fitted using a difference-of-Gaussians model (Enroth-Cugell et al., 1983) to determine the spatial arrangement of S and/or L+M inputs to the receptive field center and surround. Details and application of this model have been described previously (Dacey et al., 2000; McMahon et al., 2004; Wool et al., 2018).

Computing three-dimensional color tuning of ganglion cells. To measure cells' high-dimensional color tuning (i.e., beyond S, L–M, or L+M), we used a set of slow-modulating sinusoidal stimuli (Sun et al., 2006). These stimuli were constructed from a three-dimensional color space, *xyz*, defined by the three classical postreceptoral mechanisms of LGN neurons: a cone-subtractive (L–M) x axis, an S-cone isolating y axis, and a cone-additive (L+M) z axis (Derrington et al., 1984). When the chromaticity of a full-field stimulus is modulated around circles in the three planes formed by these axes, it can be decomposed into three phase-shifted cone-isolating sinusoids: in the isoluminant L–M versus S (*xy*) plane, L and M cones are in antiphase and are modulated 90° out of phase with S; in the L–M versus L+M (*xz*) plane, L and M are modulated 90° out of phase with each other; and in the S versus L+M (*yz*) plane, L and M are in phase but 90° out of phase with S. In any stimulus plane, vectors in the first and third quadrants represent additive input from the two mechanisms, whereas vectors in the second and fourth quadrants represent opponent inputs. Maximal cone contrast at the axes of the three stimulus planes was 8% L, 10% M, and 28% S (*xy*); 13% L, 14% M, and 0% S (*xz*); and 29% L, 29% M, 90% S (*yz*).

Each stimulus was presented as a uniform field (800–1200 µm) encompassing the cell's receptive-field center and surround. Chromaticity was modulated at 1 Hz (360°/s, or 6°/frame) in a clockwise (CW) and a counterclockwise (CCW) direction, averaged to prevent response latency from biasing the time (and, thus, angle) of maximum response. Peristimulus time histograms (PSTHs, binwidth = 12°) for both directions were constructed from the average spike rate across 12–24 stimulus presentations. We performed Fourier analysis on each CW and CCW PSTH, and computed a response vector from the amplitude and phase of the first Fourier harmonic (F1). The cell's preferred vector in a given plane was reported as the mean of the CW and CCW response vectors.

The strength of each cell's responsiveness to the L–M (x), S (y), and L+M (z) chromatic mechanisms was determined by first decomposing its preferred vector (A, θ) in each stimulus plane (*ISO*: *xy*; *LvM*: *xz*; *SvLM*: *yz*) into two axis components (x and y, x and z, or y and z) using Eqs. 2–4:

$$x_{ISO} = A_{ISO} \cos \theta_{ISO} \, , \, y_{ISO} = A_{ISO} \sin \theta_{ISO}$$

[Equations 1–2]

$$x_{LvM} = A_{LvM} \sin \theta_{LvM} \, , \, z_{LvM} = A_{LvM} \cos \theta_{LvM}$$

[Equations 3–4]

$$y_{SvLM} = A_{SvLM} \cos \theta_{SvLM} \, , \, z_{SvLM} = A_{SvLM} \sin \theta_{SvLM}$$

[Equations 5–6]

In these equations, θ_{ISO}, θ_{LvM}, *and* θ_{SvLM} are the preferred vector angles in the three planes, and x, y, and z values are the weights of each component in each two-dimensional plane. For each pair of components in Eqs. 1–6, effective contrast along stimulus axes was equalized by correcting one component by the contrast ratio between axes [e.g., $x_{ISO} \times (C_{yISO}/C_{xISO})$]. Finally, to compute the [X,Y,Z] vector projection in three-dimensional color space (where X is the total contribution of the L–M mechanism, Y is the total contribution of the S mechanism, and Z is the total contribution of the L+M mechanism), each vector component was normalized by the total contrast of the stimulus plane, C, and preferred vector amplitude, A. Since each component is doubly represented across the three total stimuli, the weights of each component were averaged over the number of component measurements, n. For a cell where all three stimulus planes were run (146 cells), $n = 2$ for each component, while for some cells where only two of the three total stimulus planes were run (83 cells), $n = 1$ for two of the three components. We found computing a component's weight to be reliable irrespective of one or two component measurements.

$$X = \frac{1}{n_x}\left[\frac{x_{ISO}A_{ISO}}{C_{ISO}} + \frac{x_{LvM}A_{LvM}}{C_{LvM}}\right]$$

[Equation 7]

$$Y = \frac{1}{n_y}\left[\frac{y_{ISO}A_{ISO}}{C_{ISO}} + \frac{y_{SvLM}A_{SvLM}}{C_{SvLM}}\right]$$

[Equation 8]

$$Z = \frac{1}{n_z}\left[\frac{z_{LvM}A_{LvM}}{C_{LvM}} + \frac{z_{SvLM}A_{SvLM}}{C_{SvLM}}\right]$$

[Equation 9]

[X,Y,Z] coordinates were converted to spherical coordinates, and reported as azimuth (φ, 0–360° on the XY isoluminant plane) and absolute value of elevation (θ, 0–90°, where 0° falls on the XY plane and 90° falls orthogonal to it, along the Z axis).

Results

We identified and recorded extracellular spiking activity from 404 retinal ganglion cells (28 blue ON, 281 OFF midget, 95 ON midget) in 37 retinae from male and female monkeys (*Macaca nemestrina, Macaca fascicularis*, or *Macaca mulatta*), targeting near-peripheral locations. As inputs to midget ganglion cells increase as a function of eccentricity (Wool et al., 2018), cells in our recording locations sample anywhere from 3 to 12 cones, theoretically maximizing the likelihood of

encountering an S-cone in a cell's receptive field. Manual receptive-field mapping was used as a first-pass approach to differentiate midget ganglion cells from their larger (2–3x) blue ON counterparts, then we used a range of stimuli to characterize each cell's cone-specific inputs, spatial properties, and chromatic signature. While our aim was to record all cells' responses to the full set of stimuli, this was not always possible; thus partial characterizations are also reported and the number of cells recorded during each stimulus is indicated. When possible, we reported recording locations in units of temporal equivalent eccentricity. Cells were located on the range of 9–48° (30±7°, n = 331). All descriptive statistics denote mean±std unless otherwise noted, and directional statistics are employed to describe circular data (Berens, 2009). Student's t tests were used to compare populations or distributions unless nonparametric data were assumed, in which case the two-sample Kolmogorov-Smirnov test was applied. All analyses were completed in MATLAB R2015b (The Mathworks).

Characterizing ganglion-cell subtypes and identifying putative S-cone input. We recorded extracellular spikes from a total of 327 retinal ganglion cells in near peripheral retina (28 blue ON cells, 222 OFF midgets, and 77 ON midgets) while presenting high-contrast S-cone or (L+M)-cone isolating stimuli (spots of 150 or 400 μm diameter, 61% contrast) to each cell's receptive-field center. While initial receptive-field mapping easily distinguished blue ON cells from midget ganglion cells by receptive-field size, blue ON cells were moreover characterized by a vigorous response to S-cone stimulation. To these square-wave stimuli, responses to S-cone stimulation was entirely absent in most ON and OFF midget cells, and these cells were instead more reliably characterized by the phase of their response to (L+M) stimulation: ON cells responded in the ON phase (0–250 ms, or ~0°) of the stimulus (Fig. 1A), while OFF cells responded in the OFF phase (250–500 ms, or ~180°; Fig. 1B). In comparison, blue ON cells reliably responded to S-cone stimulation in the ON phase, and responded to (L+M)-cone stimulation in the OFF phase (Fig. 1C). Notably, in a small subset of OFF midget cells, the characteristic OFF response to (L+M)-cone stimulation was accompanied by a small but nonetheless consistent response to S-cone stimulation in the same phase (Fig 1D).

To compare the relationship of S- and (L+M)-cone response properties of blue ON, ON midget, and OFF midget ganglion cells (including any midget ganglion cells with putative S-cone input), component mechanism–specific responses R_S and R_{L+M} were computed from the amplitude (A) and phase (θ) of spike activity during S and (L+M) stimulation (see Methods), and then plotted (L+M, x axis; S, y axis) to determine the relative strength of each mechanism. Blue ON, midget OFF, and midget ON cells form distinct clusters based on their relative responsiveness to S- or (L+M)-cone stimulation (Fig. 1E). ON and OFF midget cells are well defined by the sign of response to L+M stimulation (OFF: R_{L+M} = –28.4±16.9 spikes s^{-1}, ON: R_{L+M} = 24.9±16.1 spikes s^{-1}), and most cells' lack of response to S-cone stimulation caused clustering at the x axis (OFF: R_S = –1.1±0.90 spikes s^{-1}, ON: R_S = 0.51±0.83 spikes s^{-1}). Blue ON cells showed balanced and opponent S-ON and (L+M)-OFF responses (R_S = 30.5±14.5 spikes s^{-1}, R_{L+M} = –24.0±12.0 spikes s^{-1}). While most ON and OFF midget cells showed no S-cone response, the small subpopulation that did (OFF cells, in particular) fall farther off the x axis. We classified as putative S-cone midgets those cells with $|R_S| > 3.5$ spikes s^{-1}. This cursory criterion identified a subset of 35 S-cone midget cells (29 OFF midgets and 6 ON midgets). For most cells in this subset (26 OFF midgets, 3 ON midgets), responses to S-cone stimulation occurred in the same phase as responses to L+M stimulation (OFF: R_S = –8.2±4.0 spikes s^{-1}, R_{L+M} = –43.2±29.1 spikes s^{-1}; ON: R_S = 4.7±1.1 spikes s^{-1}, R_{L+M} = 28.2±14.8 spikes s^{-1}) suggesting that they receive excitatory S-cone input to the receptive-field center alongside their more typical L- and M-cone inputs. The remaining cells (3 OFF midgets, 3 ON midgets) showed S-cone responses in the opposite phase, suggesting an infrequently observed S-cone input to the receptive-field surround.

Spatial extent of S-cone inputs to S-OFF midgets. The S-OFF response we observed in a subset of OFF midget cells is consistent with previous anatomical and physiological studies showing that S

cones contribute via an excitatory bipolar input to the receptive field center (Klug et al., 2003; Field et al., 2010; Tsukamoto and Omi, 2015)(Dacey, 2017). We further explored this hypothesis by characterizing the spatial properties of these cells to understand how S-cone input was localized to the receptive field. For 145 midget ganglion cells (114 OFF midgets, 12 ON midgets, 19 S-OFF midgets) we measured spike discharges to (L+M)-cone and/or S-cone drifting gratings of increasing spatial frequency. Spatial tuning curves were fit with a difference-of-Gaussians function and then the frequency of peak response, f_{peak}, and the cutoff frequency, f_{cutoff} (defined as the frequency at which response amplitude decreases to $1/\sqrt{2}$ of the maximum) were computed for each cell for each stimulus. For a cell, $f_{cutoff} > f_{peak}$ indicates inputs are more localized to the receptive-field center (i.e., tuned to high spatial frequencies), while $f_{cutoff} < f_{peak}$ indicates inputs are localized to the larger receptive-field surround (i.e., tuned to high spatial frequencies).

While S-OFF cells' sensitivity to S-cone stimulation encourages an initial comparison to blue ON cells, the retina's more well-known substrate for S-cone signals, we found the spatial tuning of S-OFF midgets to be qualitatively different from the spatial tuning of blue ON cells, suggesting a functional asymmetry in how S-cone signals are transmitted across the two ganglion-cell subclasses (Figure 2). While blue ON cells show low-pass tuning to both (L+M)- and S-cone gratings with a clear antiphase relationship between mechanisms (this is due to spatially coextensive receptive fields; see (Crook et al., 2009)) (Figure 2A), S-OFF midgets showed different spatial and phasic properties to (L+M)- and S-cone gratings (Figure 2B), with a spatial profile much more similar to other OFF midget cells.

In response to L+M drifting gratings, all OFF, ON, and S-OFF midget cells showed characteristic band-pass tuning; thus, $f_{cutoff} > f_{peak}$ for all cells (Figure 2C). For OFF midget cells without S input, f_{peak} = 1.02±0.56 cpd and f_{cutoff} =2.23±0.75 cpd. For ON midget cells, f_{peak} = 0.65±0.37 cpd and f_{cutoff} =1.65±0.44 cpd. The slightly lower spatial tuning of ON midget cells has been previously described, and is attributed to slightly larger dendritic trees (Watanabe and Rodieck, 1989; Dacey, 1993). By comparison, S-OFF midget cells showed a similar spatial profile to OFF midget cells in response to L+M drifting gratings, with f_{peak} = 1.08±0.43 cpd and f_{cutoff} =2.30±0.61 cpd. Neither f_{peak} nor f_{cutoff} was statistically significantly different between OFF midget cells with or without S-cone input (p=0.65 and p=0.73, respectively; Student's t test). As expected, the phase of response to L+M drifting gratings between ON and OFF midget cells differed by ~180° (ON = 75.5±34.8°, OFF = 216.2±33.2°). In S-OFF midget cells, we found the phase of response to L+M drifting gratings (224.8±40.9°) to closely align with that observed in other OFF midget cells; no statistically significant difference of response phase was found between the two populations (p = 0.31; Student's t test) (Figure 2D).

While the spatial tuning and phase of L+M inputs to S-OFF midget cells closely resemble those of typical OFF midget cells, we also characterized the spatial tuning and phase properties of their S-cone sensitivity using S-cone drifting gratings (14 S-OFF cells). In contrast to the band-pass tuning curves observed for L+M drifting gratings, responses to S drifting gratings showed low-pass spatial tuning and were thus best fit with a single Gaussian function. The cutoff frequency of most S-OFF cells during S-cone stimulation (f_{cutoff} = 2.79±1.33 cpd) was greater than the peak frequency as identified during L+M stimulation (Figure 2E), suggesting an arrangement of S-cone inputs with high spatial frequency tuning and thus sequestered to the receptive-field center. This is further supported by the phase of response to S-cone drifting gratings we observe in these cells (218.5±43.9°), which closely matches the response phase of both S-OFF and OFF midget cells during presentation of L+M drifting gratings. This S-cone spatial profile of S-OFF cells that we describe—low-pass tuning, high f_{cutoff}, and a response phase similar to other OFF cells—strongly confirms the hypothesis that the S-cone contribution we observe in these cells is via an excitatory bipolar input to the receptive field center, with a very weak and/or infrequent contribution from the receptive-field surround.

Relating S-cone signals to L- versus M-cone opponency. After identifying a subgroup of S-OFF midget cells and characterizing the spatial properties of the S-cone input, we then asked how this input was related to the classical L–M color opponency observed in the midget pathway, and thus sought to determine whether the S-cone response had any systematic relation to the sign of either the L or M cone input to the receptive field. To answer this, we recorded extracellular spikes from 332 ganglion cells (10 blue ON cells, 256 midget OFF cells, 66 midget ON cells) during full-field L-, M-, and S-cone-isolating stimulation with square-wave stimuli (18% contrast, 800 or 1200 µm diameter), then computed the component mechanism–specific responses R_L, R_M, and R_S from each cell's F1 amplitude (A) and phase (θ). To compare the proportional strength of L-, M-, and S-cone inputs to each cell, responses were normalized as $\overline{R_L} = R_L/|R_L| + |R_M| + |R_S|$, $\overline{R_M} = R_M/|R_L| + |R_M| + |R_S|$, and $\overline{R_S} = R_s/|R_L| + |R_M| + |R_S|$.

Midget cells were characterized as cone-opponent or nonopponent by comparing the sign of $\overline{R_L}$ and $\overline{R_M}$. ON and OFF midget cells were considered opponent when L- and M-cone responses differed in sign (e.g., $-\overline{R_L}, +\overline{R_M}$ or $+\overline{R_L}, -\overline{R_M}$), and nonopponent when responses had the same sign (e.g., $+\overline{R_L}, +\overline{R_M}$ or $-\overline{R_L}, -\overline{R_M}$). Consistent with our previous recordings in near-peripheral retina (Wool, 2018), our midget cell population was heterogeneously composed of both L–M opponent (195 OFF, 44 ON) and nonopponent (61 OFF, 22 ON) cells (Figure 3A). Comparing the relative unsigned proportion of S-, L-, and M-cone inputs to each cell, we observed a distinct cluster of blue ON cells in which S-cone input comprised the majority of cone input (0.70±0.19), against nonopponent L- and M-cone inputs. By comparison, we found midget cells formed a broad continuum of L–M opponency, but also of S-cone sensitivity, particularly in OFF midget cells. The mean proportional S-cone input across ON midget cells was 0.04±0.05, while across OFF midget cells the proportion was twice as high, 0.08±0.09. The stronger overall S-cone contribution to OFF midget receptive fields is visualized in Figure 3A as a greater scatter of OFF midget cells into the orthogonal S axis; ON midget cells, by contrast, remain more closely clustered along the diagonals between the dominant L and M axes. To quantify this tendency of OFF midget cells to exhibit stronger S-cone input than ON midget cells, we compared the cumulative distributions of ON and OFF midget cells as a function of unsigned proportional S-cone input, $|\overline{R_S}|$ (Figure 3B). ON midget cells show a narrower distribution around weak or absent S-cone input, while S-cone input in OFF midget cells is more broadly distributed toward higher values of $|\overline{R_S}|$. This distribution of S-cone input between ON and OFF midget cells was statistically significantly different (Kolmogorov–Smirnov test, p = 0.0013). Indeed, a much larger percentage of OFF midget cells showed proportional S-cone input of >0.10: 27.3% (70/256), compared to 10.6% (7/66) of ON midget cells.

Nonopponent S-OFF midget cells were much more prevalent in our sample compared to opponent S-OFF cells. OFF midget cells with proportional S-cone input of >0.10 comprised 45.9% (28/61) of all nonopponent OFF cells, but only 21.5% (42/195) of opponent OFF cells. Since the likelihood of encountering opponent or nonopponent cells is itself a function of eccentricity (Wool et al., 2018), we assessed whether this difference in detectable S-cone input between opponent and nonopponent OFF cells could also be attributed to a difference in retinal location. We found the mean eccentricity between these groups to be statistically indistinguishable (nonopponent cells: 33.3±6.6°, n = 24; opponent cells: 30.7±6.8°, n = 34, Student's t-test, p = 0.15). While we did not further test whether nonopponent OFF cells have a greater likelihood of exhibiting S-cone input, the effect at least appears to be independent of eccentricity-dependent receptive-field sampling of the cone mosaic. In any case, our analysis of cone-specific inputs to midget cells demonstrated that a substantial number of both opponent and nonopponent OFF midget cells exhibit not only classical L- and M-cone inputs, but in fact input from all three cone types. As the degree of L, M, and S sensitivity manifests heterogeneously across this class of S cone–sensitive cell, we sought to further probe these interactions by assigning a precise chromatic signature to each cell, identifying where these cells would fall in a complex, three-dimensional color space.

Three-dimensional color tuning of S-OFF midget cells. A major goal of this study was to determine how the three classical postreceptoral color mechanisms (as identified in LGN neurons) (Derrington et al., 1984) combine at the level of the midget ganglion-cell receptive field to encode color sensitivity beyond L–M ('red-green') opponency. In a three-dimensional color space, *xyz*, defined by a cone-subtractive (L–M, *x*) axis, an S-cone isolating (*y*) axis, and a cone-additive (L+M, *z*) axis, classical 'red-green' opponent midget cells would simply project along the single L–M dimension. While we did observe many cells with such classical opponency, we also observed many midget ganglion cells with unbalanced L and M inputs, nonopponent L and M inputs, or even S-cone inputs (Figure 3). We thus would expect the color preferences of these cells to be heterogeneous and higher-dimensional than the single L–M opponent axis.

To assess the strength of the three postreceptoral mechanisms in individual ganglion cells, and visualize their color preferences in this three-dimensional color space, we used a set of slow-modulating sinusoidal stimuli (Sun et al., 2006) in which chromaticity was modulated around circles in three intersecting stimulus planes: an (L–M) versus S isoluminant plane (*xy*, Figure 4A), an (L–M) versus (L+M) plane (*yz*, Figure 4B), and an (L+M) versus S plane (*xz*, Figure 4C). Each stimulus was presented as a uniform field (800–1200 μm) encompassing the cell's receptive-field center and surround. For an example classical OFF midget cell with balanced and opponent L and M inputs and no S input, PSTHs show the cell's preference for –L+M stimuli in each of the three planes: near 180° (–L+M) in the *xy* plane (Figure 4D), near 135° (+M–L) in the *yz* plane (Figure 4E), and near 270° (–L–M) in the *xz* plane (Figure 4F). By contrast, an example opponent OFF midget cell with S-cone input shows significantly shifted preferred vectors that reflect not only the cell's preference for opponent –M+L stimuli, but also additional S-cone sensitivity to its receptive field: near 315° (–S, +L, –M) in the *xy* plane (Figure 4G), near 0° (+L, –M) in the *yz* plane (Figure 4H), and near 180° (–S) in the *xz* plane (Figure 4I).

We recorded spike activity from 223 retinal ganglion cells (10 blue ON cells, 191 OFF midget cells, 22 ON midget cells) during presentation of slow-modulating stimuli in the three stimulus planes. Initially, we observed that the color preferences of OFF midget, ON midget, and blue ON ganglion cells were largely heterogeneous both within and across cell type, even in response to the same color stimulus (Figure 5). As some clustering of preferred vectors was evident in each stimulus plane, we used kernel density estimation to visualize the distributions of preferred vector angles, θ, for OFF midget, ON midget, and blue ON ganglion cells (preferred vector magnitude, A, was ignored) in response to each each stimulus plane. For each cell type and stimulus plane, the distribution of preferred vector angles was binned (binwidth = 1°), convolved with a Gaussian filter (sigma = 10°), and then normalized. In the (L–M) versus S isoluminant (*xy*) plane (Figure 5, A–B), blue ON cells (n = 9) cluster closely to 90° (+S), while both ON (n = 19) and OFF midget cells (n = 183) heavily cluster at the two cone-opponent directions near 0° (+L–M) and 180° (–L+M). Notably, a small number of OFF cells show variable preferred vectors that variably depart the cone-opponent axis toward 270° (–S), with a color signature opposite to blue ON cells (Figure 5A). While kernel density estimation successfully identified the bimodal distribution of ON and OFF midget cells (OFF: 172° and 2°; ON: 172° and 347°) as well as the unimodal distribution of blue ON cells (101°), the low density of OFF midget cells in the intermediate directions toward –S (225–315°) underlines the overall scarcity of S-OFF cells in our population (Figure 5B).

In the (L–M) versus (L+M) (*yz*) plane (Figure 5, C–D), blue ON cells (n = 5) reliably cluster at 225°, where the (–L–M) component of these cells is maximally stimulated. ON (n = 22) and OFF (n = 186) midget cells show a very broad distribution of preferred vectors that span both cone-opponent (0°, 180°) and nonopponent (90°, 270°) directions, illustrating the heterogeneity of opponent responses in midget ganglion cells (e.g., (Solomon et al., 2005; Buzás et al., 2006; Martin et al., 2011; Wool et al., 2018)). The estimated preferred-vector kernels clearly identified a sharp unimodal distribution of blue ON cells (228°), and a multimodal distribution of ON and OFF midget cells: modes at two L–dominated cone-opponent directions (OFF: 194° and 327°; ON: 174° and 15°), as well as a nonzero

density for intermediate, nonopponent L-dominated +L+M (45–90°) and –L–M (225–270°) directions.

In the (L+M) versus S (*xz*) plane (Figure 5, E–F), blue ON cells (n = 10) again show a single reliable cluster near 315°, where opponent +S and –L–M mechanisms are maximally stimulated. ON midget cells (n = 13) narrowly cluster at 90° (+L+M); by contrast, OFF midget cells (n = 143) show a much broader distribution of preferred vectors that span both –L–M and –S mechanisms (Figure 5E). Compared to the bimodal distributions observed in other stimulus planes, preferred-vector kernels for ON midget, OFF midget, and blue ON cells are unimodal in the *xz* plane, but with varying broadness of their distribution. The preferred-vector kernels for blue ON cells (348°) and ON midget cells (101°) are relatively narrow and normally distributed; by contrast, while the kernel for OFF midget cells shows clear mode at 268°, there is an obvious leftward skew of the distribution, reflecting the substantial number of S-OFF cells that exhibit tuning toward the –S direction (180°) (Figure 5F).

After computing the preferred vector of each cell to each stimulus (Figure 5), we computed each cell's vector projection in three-dimensional color space (Eqs. 7–9, and Methods) and reported this in spherical coordinates: azimuth (φ, 0–360° on the *XY* plane) and absolute elevation (θ, 0–90°, where 0° lies on the *XY* plane and 90° lies on the *Z* axis). Figure 6 shows the distribution of preferred directions of all ganglion cells in three-dimensional color space. The majority of cells fall in three clusters along the azimuth: blue ON cells fall at 90° (+S), while ON and OFF midget ganglion cells plot in columns at 0° (+L–M) and 180° (–L+M). Midget cells also show variable tradeoff between being strongly L–M cone-opponent (θ = 0°) and nonopponent (θ = 90°), consistent with previous studies (e.g., (Solomon et al., 2005; Buzás et al., 2006; Field et al., 2010; Martin et al., 2011; Wool et al., 2018)). In contrast to the narrow clusters of cells at 0°, 90°, and 180°, a sparse population of OFF midget cells are widely scattered between 0° and 180°, indicating a degree of S-OFF input that varies considerably to the receptive fields of these OFF midget cells. These cells also range from strongly chromatic (L–M, θ = 0°) to strongly achromatic (L+M, θ = 90°)—this is consistent with our earlier finding that S-cone inputs are observed across both opponent and nonopponent OFF midget cells.

Discussion

While previous studies have provided anatomical and physiological evidence for an S-OFF pathway in primate retina, our characterization of S-OFF midget cells adds considerable detail to previous accounts of this putative pathway and its properties. In particular, our study shows that the contribution of S cones to OFF midget receptive fields imparts a consistent S-cone spatial profile to these cells, and broadly influences the color-sensitive properties of individual OFF midget cells, giving rise to a population with strongly heterogeneous, complex, three-dimensional color tuning.

In comparison to the anatomically distinct S-ON pathway, where specialized S-ON bipolar cells generate S-cone input to small bistratified blue ON cells (Dacey and Lee, 1994; Calkins et al., 1998), a parallel S-OFF pathway does not appear to lie within an anatomically discrete cell class. Instead, our electrophysiological recordings support the hypothesis that S-OFF signals are transmitted by the OFF midget ganglion cell circuit (Klug et al., 2003; Field et al., 2010; Tsukamoto and Omi, 2015; Dacey et al., 2017). S-OFF midget cells in the retinal near periphery demonstrate S-cone input of variable strength, but invariant phase: the OFF sign of S-cone sensitivity across all S-OFF cells is consistent with the anatomical finding that S cones contribute to OFF midget ganglion cells via OFF midget bipolar inputs to the receptive-field center. Measuring the spatial extent of S-cone input to our subset of cells supports this interpretation, as the cutoff frequency of spatial tuning curves for S-cone gratings closely matches that of tuning curves to L+M gratings in peripheral OFF midgets. This suggests that in the near periphery where midget dendritic fields accept multiple cone-bipolar inputs, L, M, and S cones all contribute to S-OFF midget ganglion cells, contrary to early characterizations of this pathway as L- and M-cone-type specific.

Early electrophysiological data do hint at this idea of an OFF midget pathway that samples L, M, and S cones to produce three-dimensional color tuning in what should otherwise be L–M opponent cells. de Monasterio et al. (1975) reported color tuning of a small percentage of opponent ganglion cells (i.e., midget cells) that did not reliably fall along the cardinal "red-green" L–M axis as previously described (Gouras, 1968; De Monasterio and Gouras, 1975): their reports of subtypes tuned to "red-cyan" and "green-magenta" strongly suggest a short-wavelength contribution to the chromatic tuning of those midget cells. Later work by Tailby et al (2008a) in near-peripheral LGN recordings (4–15° eccentricity) showed that for S+ cells, L- and M-cone sensitivity was in-phase (consistent with input from blue ON small-bistratified cells), while for S– cells, L- and M-cone sensitivity was anti-phase—consistent with our finding of a subpopulation of S-OFF midget cells that possess classical L–M opponency atop a preference for S-cone decrements.

Compared to the consistent S versus (L+M) tuning we observed in blue ON cells, the chromatic properties of S-OFF midget cells that we recorded were highly heterogeneous. While these cells respond reliably to S-cone decrements, the putative arrangement of L and M cones elsewhere in the receptive field produced cells with sensitivity to L and M cones in the same or opposite phase: that is, some cells with a (L+S)-OFF, M-ON preference (sensitivity to L cones was in phase S cones), a (M+S)-OFF, L-ON preference (sensitivity to M cones was in phase with S cones), or a (L+M+S)-OFF preference (sensitivity to all cone types was in the same phase). The heterogeneity of phase relationships observed across L, M, and S cone mechanisms in S-OFF midget cells may explain the heterogeneity of opinion on which intermediate or 'noncardinal' axis dominates postretinal chromatic sensitivity: some imaging and psychophysical studies have declared S-cone input to be synergistic with the L-cone input (e.g., (Stromeyer et al., 1998; Goddard et al., 2010; Danilova and Mollon, 2012)), while others have declared S-cone input must be synergistic with the M-cone input (e.g., (Conway, 2001; Solomon and Lennie, 2005; Horwitz et al., 2007; Lafer-Sousa et al., 2012)). In many of these studies, the use of modulating ON-OFF gratings assumes symmetry between the poles of various color axes, making it difficult to unpack the individual contributions of putative ON and OFF mechanisms to color sensitivity. It is apparent in our data that such poles are rarely symmetric and often driven by multiple cell subtypes (Figure 5, A–C). In any case, our findings suggest that any reported 'tilt' off the cardinal L–M axis can be attributed to the mixed color properties of S-OFF midget cells in retina (Figure 5A), or to the similarly heterogeneously tuned population of downstream S– cells in LGN ((Tailby et al., 2008a), Figure 3A).

The low density of S cones in the trichromatic cone mosaic (Curcio et al., 1991) generally supports the low incidence of S-OFF midget cells we found empirically, if nonselective sampling of the mosaic is assumed (Wool et al., 2018). Midget-bipolar circuit reconstructions in local regions of near-peripheral retina show clearly that S-cone input is variable even across neighboring OFF midget ganglion cells, in a manner seemingly dependent on the underlying cone mosaic (Tsukamoto and Omi, 2015), but it is difficult to discern from our own experiments whether S-OFF midgets completely tile the near-peripheral retina to fully sample the S-cone mosaic. If they do, we might predict that for the farthest peripheral midget cells with the largest receptive fields, the likelihood of any S-cone contact would increase, but with the caveat that the relative strength of S-cone input would decline as overall cone inputs (the majority of them L and M) increase. On the other hand, we would predict this tradeoff to be reversed more foveally, in that a sparse population of foveal OFF midget cells have "private-line" connectivity to single S cones just as they would to L or M cones, but at a rate in keeping with the density of S cones in the mosaic. Three-dimensional volume reconstructions of OFF midget bipolar cells show exactly this sort of connectivity at foveal S-cone pedicles (Klug et al., 2003; Dacey et al., 2017). Assuming cone-opponent signaling is established identically in these cells as in other foveal, cone-opponent, private-line cells (see (Wool et al., 2018)), such circuitry suggests there is a sparse population of foveal S-OFF, (L+M)-ON midget ganglion cells, an anatomically distinct circuit with a color tuning directly opposite the S-ON, (L+M)-OFF sensitivity of blue ON cells. While we did not encounter any of these cells in our own near-peripheral recordings, this subclass of cell is already apparent in the population of parafoveal S–

cells recorded in LGN by Tailby et al. ((2008a), Figure 3B). It is worth noting, however, that this proposed circuitry seems species-specific: in marmoset, S-OFF cells in LGN (Tailby et al., 2008b) do not have the same receptive-field properties as those described in macaque; moreover, OFF midget bipolar cells seem avoid contact to S-cones in marmoset retina (Lee et al., 2005).

A putative private-line foveal S-cone circuit carried by OFF midget ganglion cells suggests that single-cone resolution is possible for the S-OFF pathway. In the fovea, the measured S-cone acuity of 12–15 cpd (Stromeyer et al., 1978; Hess et al., 1989; Metha and Lennie, 2001) meets or exceeds the Nyquist limit as determined by S-cone spacing in the mosaic (Curcio et al., 1991), which is consistent with the private-line circuitry observed between single S-cones and midget ganglion cells observed anatomically (Klug et al., 2003; Dacey et al., 2017)—small bistratified cells, incidentally, show nearly one-to-one connectivity at this location as well (Kouyama and Marshak, 1992; Wassle et al., 1994; Calkins et al., 1998). Moreover, the diminished acuity observed beyond 2–3°, below what the S-cone mosaic should be able to support (Metha and Lennie, 2001), can be nicely explained by the rapid postreceptoral pooling from midget ganglion cells that emerges at this eccentricity. Results showing that spatial acuity (Zlatkova et al., 2008) and spatial summation thresholds (Vassilev et al., 2003) are similar for S-ON and S-OFF gratings at retinal locations within 5–10° (2 mm), but worse for S-OFF stimuli beyond this range, seem consistent with two discrete S-cone pathways with different eccentricity-dependent neural sampling rates.

Temporal differences between S-ON and S-OFF signaling also point to their propagation by separate and asymmetric mechanisms. While some studies observed faster responses to S-OFF stimuli than S-ON stimuli (McKeefry, 2003; Wool et al., 2015), others have reported slower, weaker S-OFF responses both psychophysically (Shinomori and Werner, 2008) and in electroretinography (Maguire et al., 2018). Such a small and sluggish S-OFF response may well be due to greater dilution of the S-cone signal carried by a small number of OFF midget cells, compared to the S-cone signal carried by the more robust, regular network of blue ON cells.

Our electrophysiological results provide strong evidence that S-OFF sensitivity is established in trichomatic retina, sparsely encoded in the OFF midget pathway. Challenging the supposition that this pathway is purely L- and M-cone-specific, S-OFF midget cells have a characteristic S-cone spatial signature and exhibit heterogeneous, three-dimensional color tuning across both L–M opponent and nonopponent cells. Downstream geniculocortical targets appear to recapitulate these complex, noncardinal color preferences; a retinal basis for such tuning may help explain psychophysical results showing sensitivity to axes intermediate to the classical L–M, S, and L+M cone mechanisms.

Acknowledgments

This work was supported by National Institutes of Health grant RR00166 to the Tissue Distribution Program of the National Primate Research Center at the University of Washington, grants EY07556 and EY13312 (to Q.Z.), grant EY06678 (to D.M.D.), and grant EY01730 (to the Vision Research Core at the University of Washington). We thank Julian Vrieslander for programming assistance, Paul Martin and Sam Solomon for advice and discussion, and Beth Peterson for technical assistance. Author contributions: L. E. W., Q. Z., and D. M. D. conceived of the study; L. E. W., O. P., Q. Z., and D. M. D. designed the experiments; L. E. W. and D.M.D. performed research; L. E. W. analyzed data; O. P. and D.M.D. contributed analytic tools; and L. E. W., Q. Z., and D. M. D. wrote the paper. Territorial acknowledgments: We acknowledge that research for this study was undertaken at institutions occupying unceded Indigenous land: the traditional territories of the Coast Salish people (specifically the Duwamish Tribe) (University of Washington) and the Lenape people (SUNY College of Optometry).

Bibliography

Banks MS, Sekuler AB, Anderson SJ (1991) Peripheral spatial vision: limits imposed by optics, photoreceptors, and receptor pooling. J Opt Soc Am A 8:1775-1787.

Baylor DA, Lamb TD, Yau KW (1979) Responses of retinal rods to single photons. J Physiol (Lond) 288:613-634.

Baylor DA, Nunn BJ, Schnapf JL (1987) Spectral sensitivity of cones of the monkey Macaca fascicularis. J Physiol (Lond) 390:145-160.

Berens P (2009) CircStat: A MATLAB Toolbox for Circular Statistics. Journal of Statistical Software 31.

Buzás P, Blessing EM, Szmajda BA, Martin PR (2006) Specificity of M and L cone inputs to receptive fields in the parvocellular pathway: random wiring with functional bias. J Neurosci 26:11148-11161.

Calkins DJ (2000) Representation of cone signals in the primate retina. J Opt Soc Am A 17:597-606.

Calkins DJ, Tsukamoto Y, Sterling P (1998) Microcircuitry and mosaic of a blue-yellow ganglion cell in the primate retina. J Neurosci 18:3373-3385.

Conway BR (2001) Spatial structure of cone inputs to color cells in alert macaque primary visual cortex (V-1). J Neurosci 21:2768-2783.

Crook JD, Manookin MB, Packer OS, Dacey DM (2011) Horizontal cell feedback without cone type-selective inhibition mediates "red-green" color opponency in midget ganglion cells of the primate retina. J. Neurosci 31:1762-1772.

Crook JD, Davenport CM, Peterson BB, Packer OS, Detwiler PB, Dacey DM (2009) Parallel ON and OFF cone bipolar inputs establish spatially coextensive receptive field structure of blue-yellow ganglion cells in primate retina. J Neurosci 29:8372-8387.

Curcio CA, Allen KA, Sloan KR, Lerea CL, Hurley JB, Klock IB, Milam AH (1991) Distribution and morphology of human cone photoreceptors stained with anti-blue opsin. J Comp Neurol 312:610-624.

Dacey D, Packer OS, Diller L, Brainard D, Peterson B, Lee B (2000) Center surround receptive field structure of cone bipolar cells in primate retina. Vision Res 40:1801-1811.

Dacey DM (1993) The mosaic of midget ganglion cells in the human retina. J Neurosci 13:5334-5355.

Dacey DM, Lee BB (1994) The "blue-on" opponent pathway in primate retina originates from a distinct bistratified ganglion cell type. Nature 367:731-735.

Dacey DM, Wool LE, Packer O, Wong RO (2017) Confirmation of an S-OFF midget ganglion cell pathway using serial block-face scanning electron microscopy. J Vis 17.

Danilova MV, Mollon JD (2012) Cardinal axes are not independent in color discrimination. J Opt Soc Am A 29:A157.

Dartnall H (1972) Photosensivity. In: Handbook of Sensory Physiology, pp 122-145.

De Monasterio FM, Gouras P (1975) Functional properties of ganglion cells of the rhesus monkey retina. J Physiol 251:167-195.

De Monasterio FM, Gouras P, Tolhurst DJ (1975) Trichromatic colour opponency in ganglion cells of the rhesus monkey retina. J Physiol 251:197-216.

Derrington AM, Krauskopf J, Lennie P (1984) Chromatic mechanisms in lateral geniculate nucleus of macaque. J Physiol 357:241-265.

Enroth-Cugell C, Robson JG, Schweitzer-Tong DE, Watson AB (1983) Spatio-temporal interactions in cat retinal ganglion cells showing linear spatial summation. J Physiol 341:279-307.

Field GD, Gauthier JL, Sher A, Greschner M, Machado TA, Jepson LH, Shlens J, Gunning DE, Mathieson K, Dabrowski W, Paninski L, Litke AM, Chichilnisky EJ (2010) Functional connectivity in the retina at the resolution of photoreceptors. Nature 467:673-677.

Goddard E, Mannion DJ, McDonald JS, Solomon SG, Clifford CW (2010) Combination of subcortical color channels in human visual cortex. J Vis 10:25.

Gouras P (1968) Identification of cone mechanisms in monkey ganglion cells. J Physiol 199:533-547.

Hess RF, Mullen KT, Zrenner E (1989) Human photopic vision with only short wavelength cones: post-receptoral properties. J Physiol 417:151-172.

Horwitz GD, Chichilnisky EJ, Albright TD (2007) Cone inputs to simple and complex cells in V1 of awake macaque. J Neurophysiol 97:3070-3081.

Klug K, Herr S, Ngo IT, Sterling P, Schein S (2003) Macaque retina contains an S-cone OFF midget pathway. J Neurosci 23:9881-9887.

Kolb H, Goede P, Roberts S, McDermott R, Gouras P (1997) Uniqueness of the S-cone pedicle in the human retina and consequences for color processing. J Comp Neurol 386:443-460.

Kouyama N, Marshak DW (1992) Bipolar cells specific for blue cones in the macaque retina. J Neurosci 12:1233-1252.

Lafer-Sousa R, Liu YO, Lafer-Sousa L, Wiest MC, Conway BR (2012) Color tuning in alert macaque V1 assessed with fMRI and single-unit recording shows a bias toward daylight colors. J Opt Soc Am A Opt Image Sci Vis 29:657-670.

Lee S, Grünert U (2007) Connections of diffuse bipolar cells in primate retina are biased against S-cones. J Comp Neurol 502:126-140.

Lee SC, Telkes I, Grunert U (2005) S-cones do not contribute to the OFF-midget pathway in the retina of the marmoset, Callithrix jacchus. Eur J Neurosci 22:437-447.

Maguire J, Parry NRA, Kremers J, Murray IJ, McKeefry D (2018) Human S-cone electroretinograms obtained by silent substitution stimulation. J Opt Soc Am A Opt Image Sci Vis 35:B11-B18.

Mariani AP (1984) Bipolar cells in monkey retina selective for the cones likely to be blue-sensitive. Nature 308:184-186.

Martin PR, Blessing EM, Buzás P, Szmajda BA, Forte JD (2011) Transmission of colour and acuity signals by parvocellular cells in marmoset monkeys. J Physiol 589:2795-2812.

McKeefry DJ (2003) Simple Reaction Times in Color Space: The Influence of Chromaticity, Contrast, and Cone Opponency. Invest Ophthalmol Vis Sci 44:2267-2276.

McMahon MJ, Packer OS, Dacey DM (2004) The classical receptive field surround of primate parasol ganglion cells is mediated primarily by a non-GABAergic pathway. J Neurosci 24:3736-3745.

Metha AB, Lennie P (2001) Transmission of spatial information in S-cone pathways. Vis Neurosci 18:961-972.

Packer OS, Verweij J, Li PH, Schnapf JL, Dacey DM (2010) Blue-yellow opponency in primate S cone photoreceptors. J Neurosci 30:568-572.

Shinomori K, Werner JS (2008) The impulse response of S-cone pathways in detection of increments and decrements. Vis Neurosci 25:341-347.

Solomon SG, Lennie P (2005) Chromatic gain controls in visual cortical neurons. J Neurosci 25:4779-4792.

Solomon SG, Lee BB, White AJR, Rüttiger L, Martin PR (2005) Chromatic organization of ganglion cell receptive fields in the peripheral retina. J Neurosci 25:4527-4539.

Stromeyer CF, 3rd, Kranda K, Sternheim CE (1978) Selective chromatic adaptation at different spatial frequencies. Vision Res 18:427-437.

Stromeyer CF, 3rd, Chaparro A, Rodriguez C, Chen D, Hu E, Kronauer RE (1998) Short-wave cone signal in the red-green detection mechanism. Vision Res 38:813-826.

Sun H, Smithson HE, Zaidi Q, Lee BB (2006) Specificity of cone inputs to macaque retinal ganglion cells. J Neurophysiol 95:837-849.

Tailby C, Solomon SG, Lennie P (2008a) Functional Asymmetries in Visual Pathways Carrying S-Cone Signals in Macaque. J Neurosci 28:4078-4087.

Tailby C, Szmajda BA, Buzas P, Lee BB, Martin PR (2008b) Transmission of blue (S) cone signals through the primate lateral geniculate nucleus. J Physiol 586:5947-5967.

Tsukamoto Y, Omi N (2015) OFF bipolar cells in macaque retina: type-specific connectivity in the outer and inner synaptic layers. Front Neuroanat 9:885-817.

Vassilev A, Mihaylova MS, Racheva K, Zlatkova M, Anderson RS (2003) Spatial summation of S-cone ON and OFF signals: effects of retinal eccentricity. Vision Res 43:2875-2884.

Wassle H, Grunert U, Martin PR, Boycott BB (1994) Immunocytochemical characterization and spatial distribution of midget bipolar cells in the macaque monkey retina. Vision Res 34:561-579.

Watanabe M, Rodieck RW (1989) Parasol and midget ganglion cells of the primate retina. J Comp Neurol 289:434-454.

Wool LE, Crook JD, Troy JB, Packer OS, Zaidi Q, Dacey DM (2018) Nonselective Wiring Accounts for Red-Green Opponency in Midget Ganglion Cells of the Primate Retina. J Neurosci 38:1520-1540.

Wool LE, Komban SJ, Kremkow J, Jansen M, Li X, Alonso J-M, Zaidi Q (2015) Salience of unique hues and implications for color theory. J Vis 15:1-11.

Zlatkova MB, Vassilev A, Anderson RS (2008) Resolution acuity for equiluminant gratings of S-cone positive or negative contrast in human vision. J Vis 8:9 1-10.

Figures

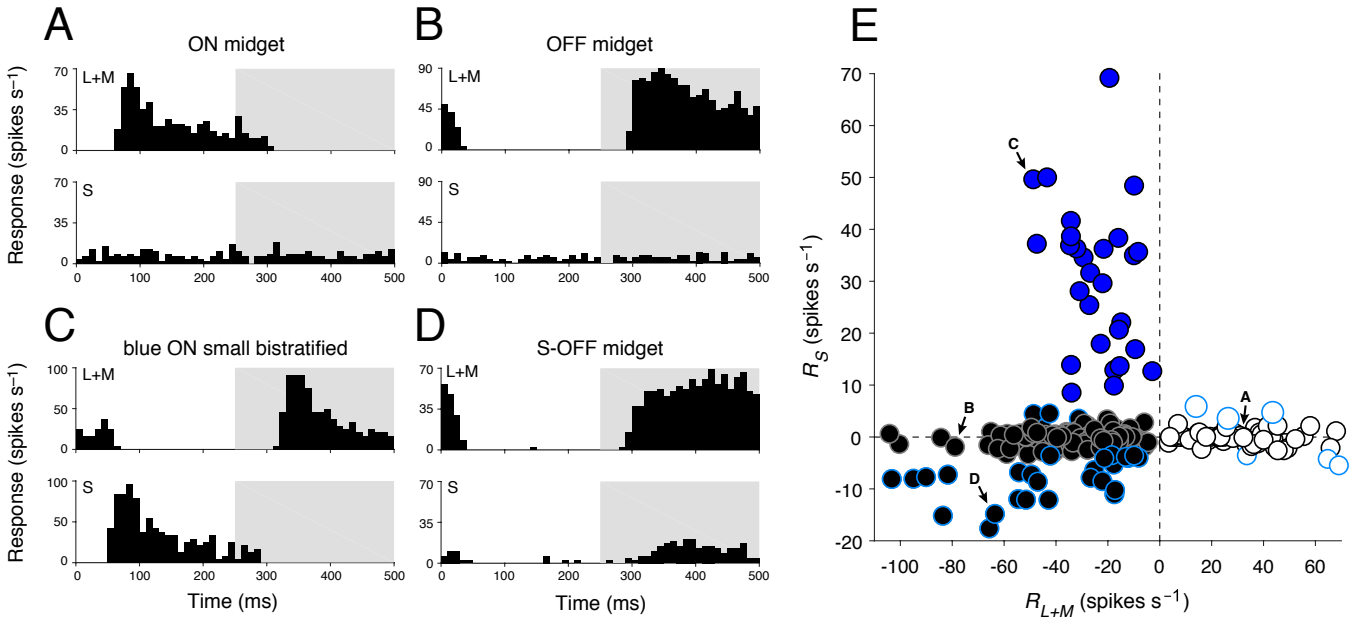

Figure 1. Cone-mechanism-specific responses in retinal ganglion cell subtypes. (A) Peristimulus time histogram of a typical ON midget ganglion cell shows spiking activity in the ON phase (0–250 ms) of a 2-Hz modulating (L+M)-cone-isolating stimulus (top) while showing no activity during a modulating S-cone-isolating stimulus (bottom). (B) A typical OFF midget cells shows the reverse behavior, with spiking activity in the OFF phase (250–500 ms) of a 2-Hz modulating (L+M)-cone-isolating stimulus (top) but also showing no activity during a modulating S-cone-isolating stimulus (bottom). (C) A blue ON ganglion cell responds to both L+M (top) and S (bottom) cone-isolating stimuli, with opponent phase. (D) An S-OFF midget ganglion cell demonstrates classical sensitivity to (L+M)-cone stimuli (top), as well as a small but stable response to S-cone stimuli (bottom); both responses occur in the OFF phase. (E) Ganglion cell types cluster based on their responsiveness S- (R_S) and (L+M)- (R_{L+M}) cone stimulation. Blue circles, blue ON cells; white circles, ON midget cells; black circles, OFF midget cells. Blue-bordered white and black circles denote midget ganglion cells with $|R_S| > 3.5$ spikes s^{-1}. Labeled cells are those shown in panels A–D, respectively.

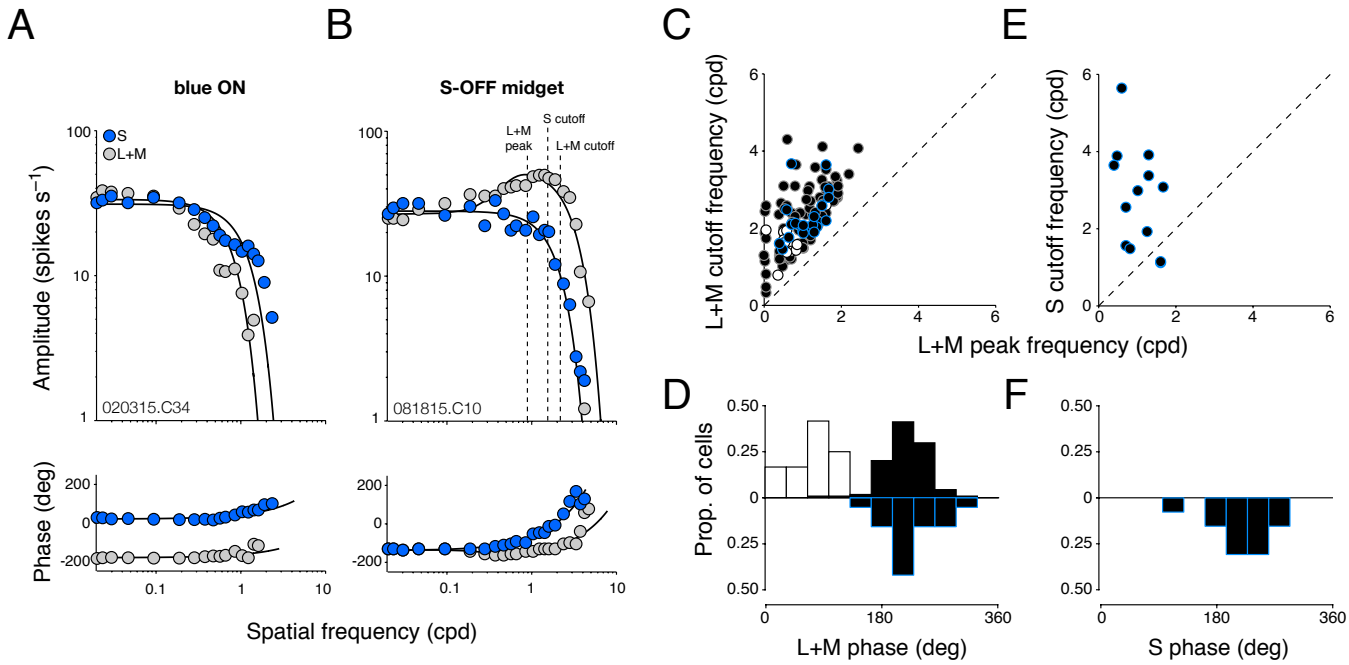

705

Figure 2. Spatial extent of S-cone input to OFF midget ganglion cells. (A,B) Compared to blue ON ganglion cells, which demonstrate spatially coextensive, low-pass, and antiphase spatial tuning to both S- and (L+M)-cone gratings (A), S-OFF midget ganglion cells demonstrate a low-pass spatial sensitivity to S-cone gratings atop the typical band-pass sensitivity to (L+M)-cone gratings, which
710 occurs in the same phase (B). (C) All midget ganglion cells demonstrated characteristic band-pass tuning to L+M gratings, in which the cutoff frequency for L+M gratings occurs at a higher spatial frequency than the peak frequency. The L+M spatial profiles of putative S-OFF midget ganglion cells (black/blue circles) are compared to typical ON (white circles) and OFF (black circles) midget cells, with cutoff frequency for L+M gratings (*y* axis) plotted as a function of peak frequency (*x*
715 axis). (D) Distribution of response phase to L+M gratings for S-OFF (black/blue histogram), ON (white bars), and OFF (black bars) midget cells. (E) For S-OFF midget cells, cutoff frequency for S gratings (*y* axis) is plotted as a function of peak frequency for L+M gratings (*x* axis). (F) Distribution of response phase to S gratings, for S-OFF midget cells.

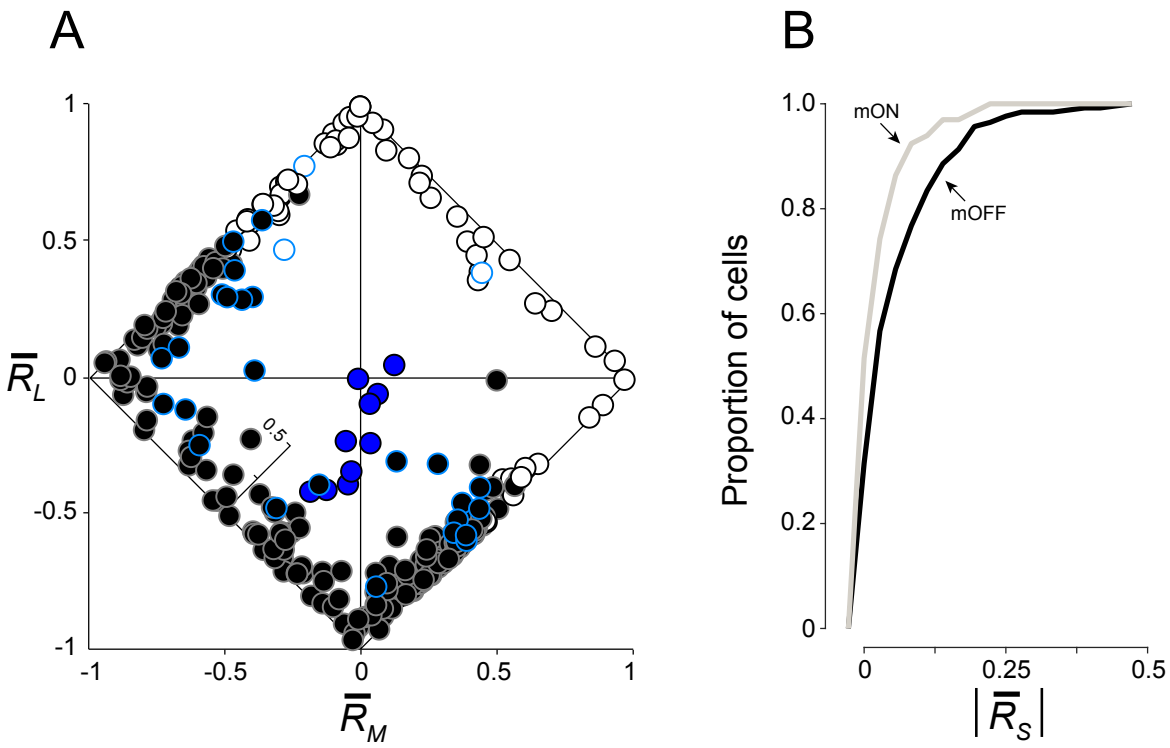

Figure 3. L-, M-, and S-cone-specific inputs to ganglion-cell subtypes. (A) Cone-specific responses R_L, R_M, and R_S are revealed for each ganglion cell by plotting relative L- versus M-cone input on the *x* and *y* axes, respectively. S-cone input is denoted by a third internal *z* axis. Classical L–M opponency is assessed by comparing the sign of R_L and R_M: opponent cells fall along the diagonals where the signs of R_L and R_M are opposed, while nonopponent cells fall along the diagonals where the signs are matched. Blue ON cells (blue circles) demonstrate sign-matched L- and M-cone inputs, along with strong S-cone input. ON (white circles) and OFF (black circles) midget cells demonstrate both opponent and nonopponent L- and M-cone inputs, with OFF midget cells demonstrating stronger S-cone input overall. Blue-bordered white and black circles denote ON and OFF midget cells initially identified as S-cone-sensitive in Figure 1. (B) Cumulative distribution of proportional S-cone input to OFF midget ganglion cells (black) compared to ON midget ganglion cells (gray).

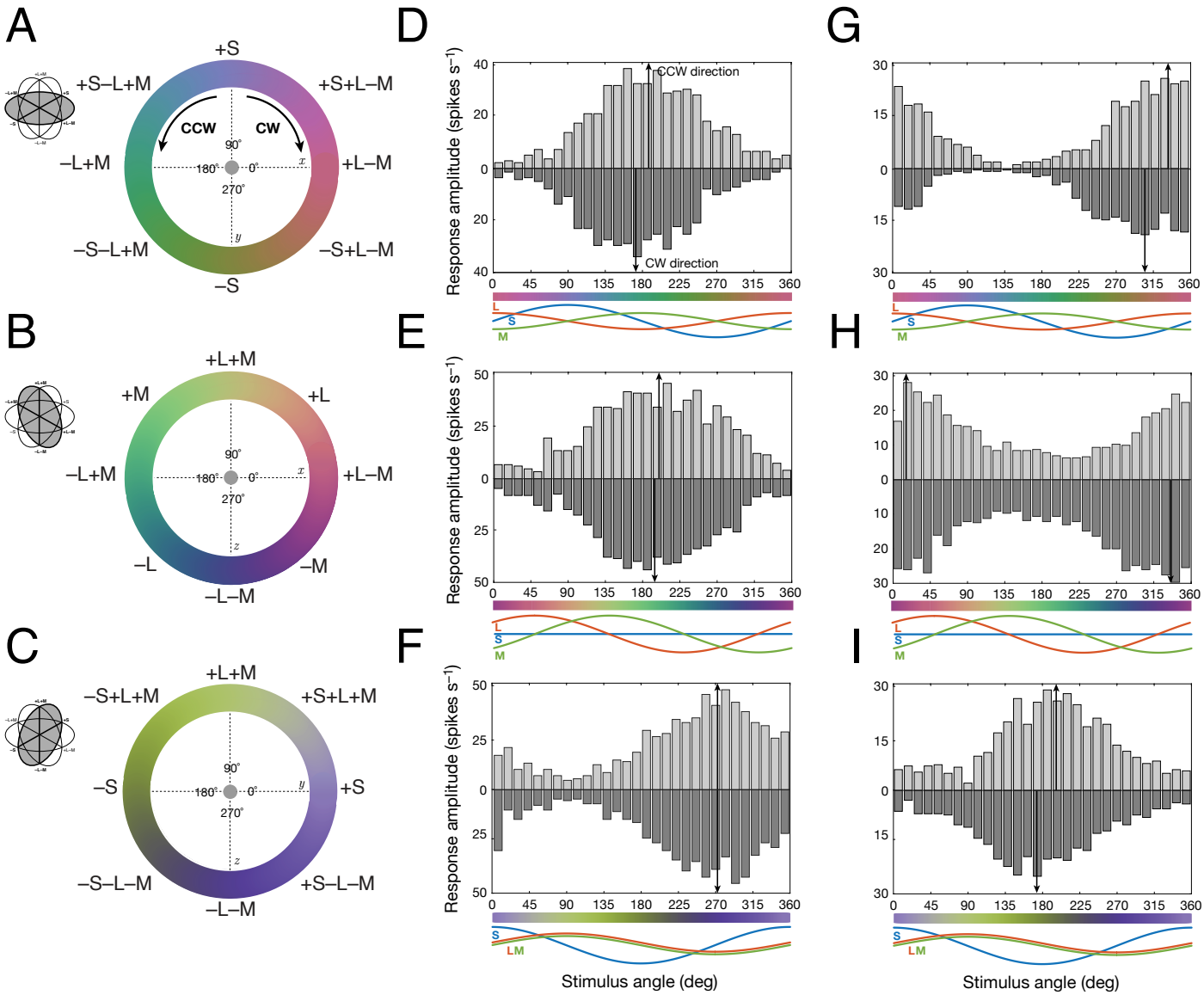

735 **Figure 4. Measuring color preferences in individual ganglion cells.** (A–C) The chromaticity of a uniform, full-field stimulus was modulated in clockwise (CW) or counterclockwise (CCW) directions along around circles in three intersecting planes of three-dimensional color space, xyz: an (L–M) versus S isoluminant plane (*xy*, A), an (L–M) versus (L+M) plane (*yz*, B), and an (L+M) versus S plane (*xz*, C). (D–F) Peristimulus time histograms reveal the color preference (angle at
740 maximum response) in each stimulus plane for a typical opponent OFF midget ganglion cell with weak/absent S-cone input: near 180° (–L+M) in the *xy* plane (D), near 135° (+M–L) in the *yz* plane (E), and near 270° (–L–M) in the *xz* plane (F). (G–I) Peristimulus time histograms reveal the color preference (angle at maximum response) in each stimulus plane for an S-OFF midget ganglion cell: near 315° (–S, +L, –M) in the *xy* plane (G), near 0° (+L, –M) in the *yz* plane (H), and near 180° (–S)
745 in the *xz* plane (I).

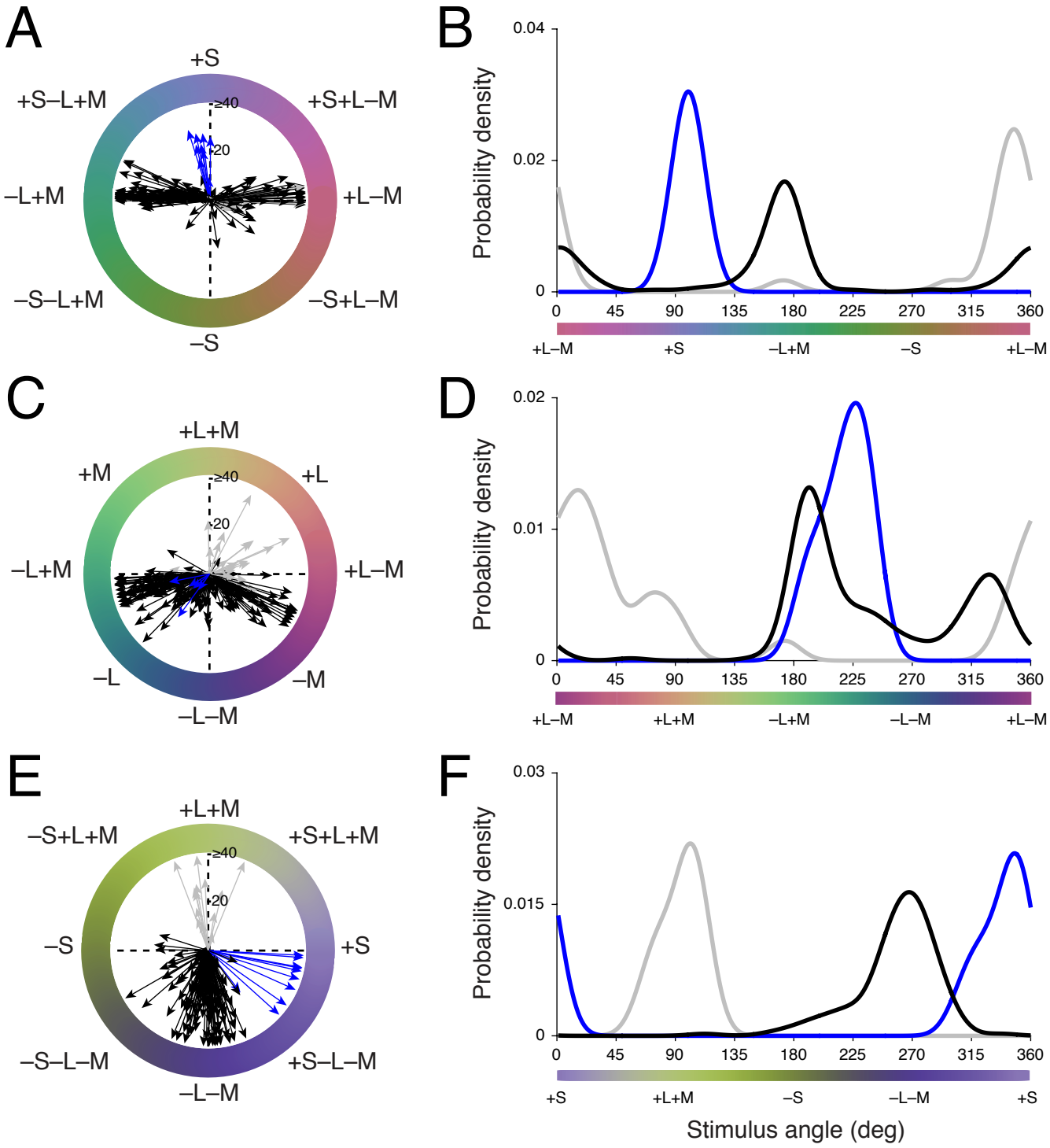

Figure 5. Distributions of color preferences across blue ON, ON midget, and OFF midget ganglion cells. (A–B) Individual preferred vectors (A) and kernel density estimation (B) for cells in the *xy* plane. (C–D) Individual preferred vectors (C) and kernel density estimation (D) for cells in the *yz* plane. (E–F) Individual preferred vectors (E) and kernel density estimation (F) for cells in the *xz* plane. Blue, blue ON cells; gray, ON midget cells; black, OFF midget cells.

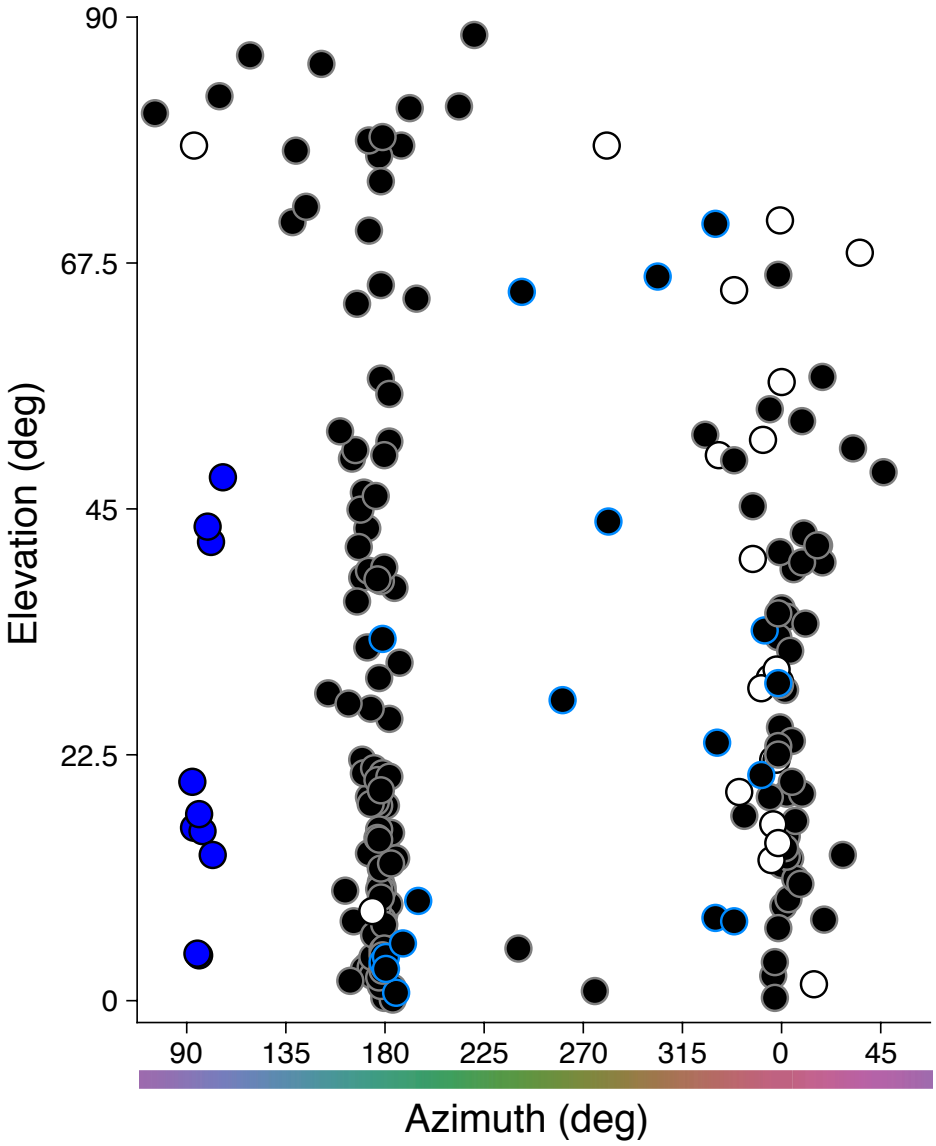

Figure 6. Three-dimensional color signatures of blue ON, ON midget, and OFF midget cells. The preferred azimuth and elevation of each cell was computed from its preferred [*X,Y,Z*] vector in Cartesian coordinates as generated from its preference across the three individual stimulus planes (Figure 5). Blue circles, blue ON cells; white circles, ON midget cells; black circles, OFF midget cells. Black/blue circles denote OFF midget cells initially identified as S-cone-sensitive in Figure 1.